

MODELING THE EFFECT OF TEMPERATURE ON OZONE-RELATED MORTALITY¹

BY ANDER WILSON^{2,*}, ANA G. RAPPOLD[†],
LUCAS M. NEAS[†] AND BRIAN J. REICH^{3,*}

*North Carolina State University** and *US Environmental
Protection Agency[†]*

Climate change is expected to alter the distribution of ambient ozone levels and temperatures which, in turn, may impact public health. Much research has focused on the effect of short-term ozone exposures on mortality and morbidity while controlling for temperature as a confounder, but less is known about the joint effects of ozone and temperature. The extent of the health effects of changing ozone levels and temperatures will depend on whether these effects are additive or synergistic. In this paper we propose a spatial, semi-parametric model to estimate the joint ozone-temperature risk surfaces in 95 US urban areas. Our methodology restricts the ozone-temperature risk surfaces to be monotone in ozone and allows for both nonadditive and nonlinear effects of ozone and temperature. We use data from the National Mortality and Morbidity Air Pollution Study (NMMAPS) and show that the proposed model fits the data better than additive linear and nonlinear models. We then examine the synergistic effect of ozone and temperature both nationally and locally and find evidence of a nonlinear ozone effect and an ozone-temperature interaction at higher temperatures and ozone concentrations.

Received December 2013; revised May 2014.

¹The research described in this article has been reviewed by the National Health and Environmental Effects Research Laboratory, US Environmental Protection Agency, and approved for publication. Approval does not signify that the contents necessarily reflect the views and policies of the Agency, nor does the mention of trade names of commercial products constitute endorsement or recommendation for use.

²Supported in part by an appointment to the Research Participation Program for the US Environmental Protection Agency, Office of Research and Development, administered by the Oak Ridge Institute for Science and Education through an interagency agreement between the US Department of Energy and EPA.

³Supported in part by the EPA (R835228) and NIH (5R01ES014843-02).

Key words and phrases. Air pollution, monotone regression, mortality, ozone-temperature interaction, semi-parametric regression, spatial modeling.

This is an electronic reprint of the original article published by the
Institute of Mathematical Statistics in *The Annals of Applied Statistics*,
2014, Vol. 8, No. 3, 1728–1749. This reprint differs from the original in pagination
and typographic detail.

The US Environmental Protection Agency (EPA) has concluded that current scientific evidence supports a “causal relationship” between ozone and respiratory health effects and a “likely to be causal” relationship between ozone and cardiovascular health effects and mortality [US EPA (2013)]. Extreme temperatures, especially heat waves, have also shown adverse associations with respiratory and cardiovascular health [Bhaskaran et al. (2009), Turner et al. (2012)]. As a photochemical air pollutant, ozone and temperature are both driven by solar radiation and their association is enhanced by the temperature dependence of other ozone precursors [Bloomer et al. (2009)]. Both ambient temperatures and ground-level ozone are expected to increase in the near future [US EPA (2009)] in response to anticipated climate changes [IPCC (2007)]. Under these circumstances, a better understanding of the joint effects of temperature and ozone on human health is essential for public health.

Most multi-city, time-series studies of ozone have focused on a main ozone effect while controlling for potential confounding variables in a generalized additive model. The highly influential analysis of Bell et al. (2004) estimated a 0.25% (0.12%–0.39%) increase in mortality associated with a 10 ppb increase in same-day mean ozone at the national level while controlling for confounders such as temperature and weather conditions. Recent studies have found evidence that the joint effects of ozone and temperature may not be additive [Bell, Peng and Dominici (2006), Smith, Xu and Switzer (2009), Chen et al. (2013)]. Future climate change scenarios predict increases in the high ends of the distributions of both the ozone and temperature. Under these future conditions, the disease burden of high ozone and temperature days may be different if the joint ozone-temperature effect is synergistic instead of additive.

Estimating the existence and nature of an interactive effect is nontrivial as temperature and ozone are both correlated with health outcomes and with each other. In multi-city, time-series studies the analysis is further complicated by the different ozone and temperature ranges observed in each city, which makes pooling estimates across cities challenging. Several studies of ozone-related daily mortality have used a stratified model to examine the potential differences in ozone effect by temperature and found a larger average ozone effect on high temperature days compared to moderate temperature days [Bell and Dominici (2008), Ren et al. (2008a), Smith, Xu and Switzer (2009)]. However, average ozone levels are higher on high temperature days (see Figure 1, e.g., and Figure 1 in the supplementary material for additional details [Wilson et al. (2014)]) and the ozone effect may be larger at higher ozone concentrations [Smith, Xu and Switzer (2009)]. This makes it unclear if the larger average ozone effect on high temperature days is due to the higher ozone on those days or an ozone-temperature interaction.

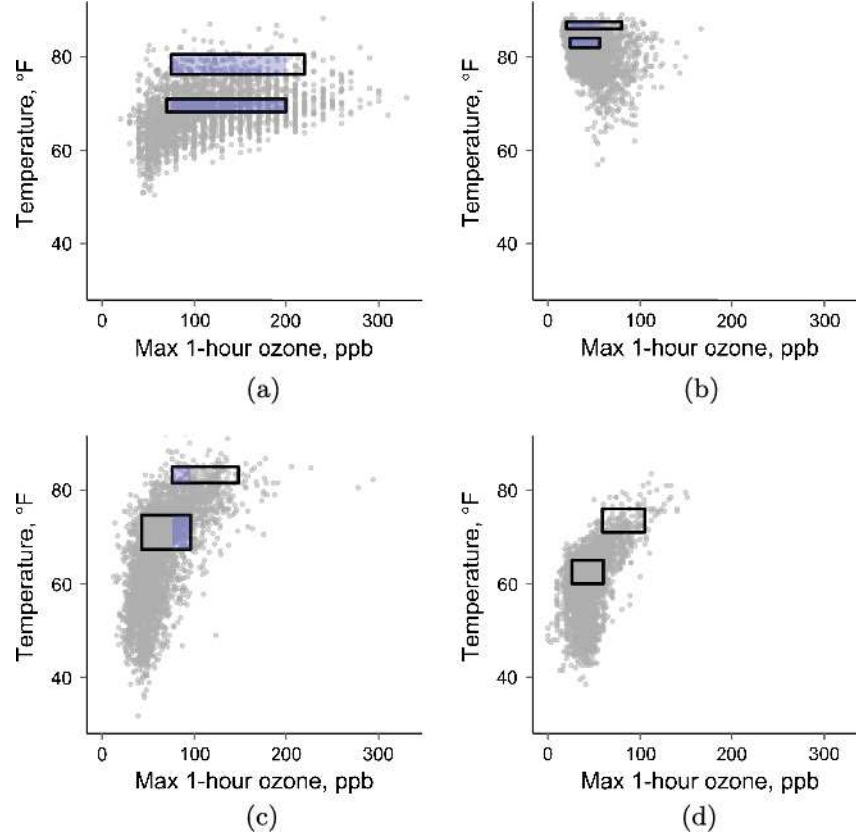


FIG. 1. Ozone-temperature distribution for selected cities. The upper and lower boxes contain data for high temperature days and moderate temperature days, respectively, over the observed ozone range. The purple subsections highlight the common ozone range, the intersection of the ozone ranges for high and moderate temperature days. Details on the definition used to identify these days are in Section 3.3. Seattle is the only city in the data set that does not have a common ozone range. (a) Los Angeles, (b) Miami, (c) New York, (d) Seattle.

To estimate interaction, the concentration-response gradient for ozone must be evaluated at different temperature ranges for the same ozone range. Matching on ozone isolates interaction from the potential confounding caused by higher ozone levels at higher temperatures and nonlinear ozone effects. One way to do this is to estimate the full ozone-temperature risk surface and evaluate the rate of change of the risk surface in the ozone direction at different temperatures for a constant ozone value. The gradient of the risk surface with respect to ozone describes the ozone effect for each temperature and ozone concentration. A changing gradient as a function of temperature for a fixed ozone value signifies interaction between ozone and temperature.

We will refer to the gradient in the ozone direction as the log relative risk (log RR) of ozone throughout, which approximates excess RR.

Recent studies have estimated the ozone-temperature risk surface in single-city and independently in multi-city analyses [Chen et al. (2013), Ren et al. (2008a)]. The risk surfaces appear to be nonlinear and nonadditive, but inference was limited to visual inspection. Instead, these studies resorted to a stratified model with different linear effects in each temperature stratum for a formal analysis instead of making quantitative inference from the risk surfaces. In addition, the multi-city approach used by Ren et al. (2008a) estimates the risk surfaces independently in each city, not allowing for sharing of information between cities. The resulting risk surface estimates are highly variable and do not allow for combining city-specific surfaces to estimate a national risk surface.

In this paper, we propose a spatial monotone surface model to estimate the ozone-temperature risk and log RR surfaces in multi-city time-series studies. We model the ozone-temperature risk surface with the outer-product of Bernstein polynomial basis functions and restrict the surfaces to be monotone in ozone. The Bernstein polynomial formulation enables closed-form representation of the risk surfaces and log RR surfaces and facilitates comparisons between cities. It also allows for sharing strength between nearby cities with a spatial model for the basis coefficients.

We also present a two-stage approach to this model that reduces its computational burden for large data [following the framework of Dominici et al. (2002)]. In the two-stage approach, we introduce a transformation that allows a different local basis expansion to be used in each city that adapts to the city-specific ozone and temperature ranges. This allows for the first-stage surface estimates to be estimated with a basis expansion specifically tailored to the ozone-temperature distribution in each city. However, the second stage surfaces use a common basis expansion spanning the national ozone-temperature distribution.

We use the proposed spatial monotone surface model to estimate the national and city-specific log RR surfaces in 95 US urban areas using data from the National Morbidity and Mortality Air Pollution Study [NMMAPS; Samet et al. (2000a, 2000b)]. Our results show evidence of a synergistic ozone-temperature effect. At higher temperatures and ozone values, the log RR of ozone tends to increase with temperature. We find the ozone-temperature interaction increases estimates of excess mortality at higher temperatures.

1. Spatial monotone surface model. We assume the mortality count Y_{ct} in city c at time t is Poisson with log mean

$$(1) \quad \log E(Y_{ct}) = f_c(\text{ozone}_{ct}, \text{temp}_{ct}) + g_c(\text{confounders}_{ct}),$$

where f_c is the city-specific ozone-temperature risk surface and g_c controls for potential confounding variables. The model for daily mortality is adopted from Bell et al. (2004) by moving daily mean temperature from the confounder model g_c to the risk model f_c and relaxing the assumptions on f_c to include interaction and nonlinear effects. The bivariate risk surface f_c is modeled with a spatial prior that imposes monotonicity in the ozone direction. The confounder model g_c includes linear and nonlinear functions of potential confounders. In the subsections below we specify models for the components of (1).

1.1. Ozone-temperature surface model. We model f_c as the outer-product of Bernstein polynomial basis expansions of ozone and temperature [Lorentz (1986), Tenbusch (1997)]. This allows for a flexible regression surface including nonlinear and nonadditive effects, but includes additive linear or polynomial effects as special cases. When making inference on a potentially nonlinear and nonadditive risk function the log of the expected change in risk at each concentration of ozone and temperature is expressed by the derivative of the log risk surface f_c . Both the Bernstein polynomial regression function (the log risk surface f_c) and its derivatives (the log RR surface) can be expressed in closed form, facilitating analysis of the log RR of ozone.

The k th Bernstein polynomial basis function of order M is $b_k(x, M) = \binom{M}{k} x^k (1-x)^{M-k}$ for $x \in [0, 1]$. Denote ozone as x_1 , temperature as x_2 and $\mathbf{x} = (x_1, x_2)^T$. To scale the data to the unit interval, we define the basis function $B_{l,k}(x_l, M) = b_k[(x_l - \min_{ct} x_{l,ct})/r_l, M]$, where $r_l = \max_{ct} x_{l,ct} - \min_{ct} x_{l,ct}$ and $l = 1, 2$ indicates ozone and temperature, respectively. For notational simplicity let $B_{j,k}(\mathbf{x}, M_1, M_2) = B_{1,j}(x_1, M_1) \times B_{2,k}(x_2, M_2)$. The bivariate regression function is

$$(2) \quad f_c(\mathbf{x}) = \sum_{j=0}^{M_1} \sum_{k=0}^{M_2} \psi_{j,k,c} B_{j,k}(\mathbf{x}, M_1, M_2),$$

where j and k index the ozone and temperature basis expansions, respectively. The first derivative of (2) with respect to ozone is

$$(3) \quad \frac{\partial f_c(\mathbf{x})}{\partial x_1} = M_1 \sum_{j=0}^{M_1-1} \sum_{k=0}^{M_2} (\psi_{j+1,k,c} - \psi_{j,k,c}) B_{j,k}(\mathbf{x}, M_1 - 1, M_2),$$

the log RR of ozone. This is the change in log expected mortality associated with a small increase in ozone.

For simplicity, we write the $(M_1 + 1)(M_2 + 1)$ -vector of unknown coefficients as

$$(4) \quad \boldsymbol{\psi}_c = (\psi_{0,0,c}, \dots, \psi_{M_1,0,c}, \psi_{0,1,c}, \dots, \psi_{M_1,M_2,c})^T.$$

Also, denote the $n_c \times (M_1 + 1)(M_2 + 1)$ basis expansion of ozone and temperature in city c over days $t = 1, \dots, n_c$ as

$$(5) \quad \mathbf{B}(\mathbf{X}_c) = [B_{0,0}(\mathbf{X}_c, M_1, M_2), \dots, B_{M_1, M_2}(\mathbf{X}_c, M_1, M_2)]^T.$$

1.2. Hierarchical model for monotonicity and spatial smoothing. We evaluate the bivariate association of current day's ambient temperature and ozone with mortality based on the prior hypothesis of a monotonic, but nonlinear, effect of ozone and a nonlinear effect of temperature. The adverse health effects of short-term exposures to ozone have been well established and described as causal to respiratory effects and likely to be causal to mortality [US EPA (2006, 2013)]. Previous studies have estimated a monotone concentration-response function using the same data without imposing specific shape restrictions [Bell, Peng and Dominici (2006), Smith, Xu and Switzer (2009)]. A monotone relationship has also been found in observational [Korrick et al. (1998), Ostro (1993)] and controlled exposure [Horstman et al. (1990), McDonnell et al. (2012)] human studies of pulmonary function. Temperature effect has been described to have “inverted J” or “U-shaped” risk function [Curriero et al. (2002)]. To reflect this prior knowledge, we constrain the ozone effect to be monotone, but leave the temperature effect unconstrained.

Bernstein polynomials are well suited for shape-restricted regression [see Chang et al. (2007), Curtis and Ghosh (2011), Wang and Ghosh (2012)]. From (3), a sufficient condition for monotonicity in the ozone direction is $\psi_{j+1,k,c} \geq \psi_{j,k,c}$ for all j and k . We reparameterize the coefficients as $\theta_{0,k,c} = \psi_{0,k,c}$ and $\theta_{j,k,c} = \psi_{j+1,k,c} - \psi_{j,k,c}$ for $j > 0$ using the matrix

$$(6) \quad \mathbf{T} = \mathbf{I}_{M_2+1} \otimes \begin{pmatrix} 1 & 0 & 0 & \cdots & 0 & 0 \\ -1 & 1 & 0 & \cdots & 0 & 0 \\ 0 & -1 & 1 & \cdots & 0 & 0 \\ \vdots & \vdots & \vdots & \ddots & \vdots & \vdots \\ 0 & 0 & 0 & \cdots & -1 & 1 \end{pmatrix}_{(M_1+1) \times (M_1+1)}.$$

With this parameterization $\boldsymbol{\theta}_c = \mathbf{T}\boldsymbol{\psi}_c$ and $f(\mathbf{x}; \boldsymbol{\theta}_c)$ is monotone in x_1 if $\theta_{j,k} \geq 0$ for $j > 0$.

The ozone-temperature surface can vary across cities. To borrow strength across nearby cities while ensuring a monotone risk surface, we model the basis coefficients with a truncated multivariate Gaussian process (GP). To do this, we define the latent vector $\boldsymbol{\theta}_c^*$ and let $\theta_{0,k,c} = \theta_{0,k,c}^*$ and $\theta_{j,k,c} = \max(0, \theta_{j,k,c}^*)$ if $j > 0$ for all k .

The prior on $\boldsymbol{\theta}_c^*$ is a multivariate Gaussian process with mean $E(\boldsymbol{\theta}_c^*) = \boldsymbol{\mu}$ and separable covariance function

$$(7) \quad \text{cov}(\boldsymbol{\theta}_c^*, \boldsymbol{\theta}_{c'}^*) = \exp\left[-\frac{d(c, c')}{\rho}\right] \times \mathbf{S}_2 \otimes \mathbf{S}_1,$$

where \mathbf{S}_1 is a $(M_1 + 1) \times (M_1 + 1)$ matrix capturing covariance in the ozone direction, \mathbf{S}_2 is a $(M_2 + 1) \times (M_2 + 1)$ matrix capturing the covariance in the temperature direction, and the exponential function captures spatial dependence. The distance function $d(c, c')$ is the great circle distance between the centers of cities c and c' in kilometers. In applications where the spatial units are all neighboring, a conditional autoregressive model [CAR; Banerjee, Gelfand and Carlin (2004), Gelfand et al. (2010), Lawson (2006)] may be a reasonable alternative to the distance-based GP. However, there are very few neighboring cities with observed data in the NMMAPS data analyzed in Section 3, so we chose the distance-based GP over the neighbor-based CAR. The mean vector $\boldsymbol{\mu}$ has prior $N(\mathbf{1}\mu_0, \tau\mathbf{S}_2 \otimes \mathbf{S}_1)$. While each component of the separable covariance is not identifiable on its own, the product is identifiable.

In many two-stage normal-normal models, $\boldsymbol{\mu}$ is often interpreted as the estimate of the national average risk [e.g., Bell et al. (2004)]; however, in this model $\boldsymbol{\mu}$ represents the mean of the latent process $\boldsymbol{\theta}_c^*$ and not the process defining the shape restricted surfaces of interest and thus does not have the same interpretation. To obtain the estimate of the national average log RR surface presented in Section 3, we use the precision weighted average of the city-specific log RR surfaces which are realizations of a truncated process $\boldsymbol{\theta}_c$ defining the modeled shape restricted surfaces. The precision weighted estimate gives more weight in the tails to cities with data extending to those regions of the surface, whereas the population weighted and unweighted cities do not reflect the different ozone-temperature distribution in each city.

1.3. Confounder model. We define g_c as a generalized additive model that includes linear and nonlinear effects for potential confounders. This is the confounder model used by Bell et al. (2004), with the same degrees of freedom, excluding daily mean temperature which is now in f_c . The confounder model includes an age-specific intercept (<65 , $65-74$, ≥ 75), categorical variables for day of week, and smooth functions of time interacted with age group with seven degrees of freedom per year (natural splines). We control for additional effects of weather with natural cubic spline of the 3-day running mean of temperature with six degrees of freedom, natural cubic spline of dewpoint with 3 degrees of freedom and of the 3-day running mean of dewpoint with 3 degrees of freedom. The confounder model can be represented as the linear model $g_c(\mathbf{Z}_c) = \mathbf{Z}_c\boldsymbol{\gamma}_c$. The prior for the confounder regression coefficients is $\pi(\boldsymbol{\gamma}_c) \propto 1$. While the prior for the risk surface f_c includes a spatial component, the prior on the confounder model is independent between cities.

2. A two-stage approach for large data sets. For large data sets, estimating the ozone-temperature risk surfaces is computationally intensive. To ease computation, we break the model into two stages, similar to the approach used by Dominici et al. (2002) and Bell et al. (2004). The two-stage approach approximates the spatial monotone model presented in Section 1 but with reduced computational burden. In the first stage, we estimate (1) separately in each city with no monotonicity constraint or spatial smoothing using computationally efficient quasi-likelihood estimation. Then, we use the first-stage parameter estimates as data for a Bayesian hierarchical model that spatially smooths the risk surfaces and constrains each city’s risk surface to be monotone in ozone. The results given in Section 3 are produced using this two-stage approach.

A natural approach for the city-specific estimates is to use the same basis expansion in each city. However, the observed ozone and temperature ranges vary dramatically from city to city. As a result, some basis functions are well supported at the national level but not supported in some cities individually. This can yield unstable first-stage estimates. To extract as much information as possible from each city in the first stage, we use a local basis expansion in each city that spans only the observed ozone and temperature ranges in that city. In the second stage a common basis expansion is used for all cities to approximate the full model described in Section 1. Figure 2 in the supplementary material shows the first and second stage basis expansions for six cities [Wilson et al. (2014)].

2.1. Stage 1: City-specific GLM regression. The first-stage basis expansions are scaled to the city-specific ozone and temperature ranges. In city c the first-stage basis functions are $b_{l,k}^c(x_l, M^c) = b_k[(x_l - \min_t x_{l,ct})/r_l^c, M^c]$, where $r_l^c = \max_t x_{l,ct} - \min_t x_{l,ct}$, for $l = 1, 2$. The first-stage estimates can also vary in the order of the basis expansion, allowing for smaller M_1^c and M_2^c in cities with smaller ozone and temperature ranges, respectively. Using this basis expansion, the first-stage model of f_c is

$$(8) \quad f_c(\mathbf{x}) = \sum_{j=0}^{M_1^c} \sum_{k=0}^{M_2^c} \beta_{c,j,k} b_{1,j}^c(x_1, M_1^c) b_{2,k}^c(x_2, M_2^c),$$

with unknown first-stage parameters $\beta_{c,j,k}$, $j = 0, \dots, M_1^c$ and $k = 0, \dots, M_2^c$. The confounder model remains as specified in Section 1.3. Denote the first-stage estimate as $(\hat{\beta}_c^T, \hat{\gamma}_c^T)^T$ and $\text{cov}[(\hat{\beta}_c^T, \hat{\gamma}_c^T)^T] = \mathbf{V}_c$, where \mathbf{V}_c can be partitioned as

$$(9) \quad \mathbf{V}_c = \begin{pmatrix} \mathbf{V}_{c,11} & \mathbf{V}_{c,12} \\ \mathbf{V}_{c,21} & \mathbf{V}_{c,22} \end{pmatrix},$$

and $\mathbf{b}_c(\mathbf{X}_c)$ is the $n_c \times (M_1^c + 1)(M_2^c + 1)$ matrix of first-stage basis expansions. We assume that $n_c > (M_1^c + 1)(M_2^c + 1)$ in all cities.

The first-stage parameters β_c correspond to different basis functions than those used in other cities and in the global expansion in (2). Hence, β_c are not directly comparable across cities or with ψ_c . This difference is resolved in the second stage (Section 2.2).

2.2. Stage 2: Bayesian model for stage 1 output. In the second stage, we reparameterize the first-stage risk surface estimates in terms of the global basis expansion (2). This provides a common set of parameters θ_c to estimate f_c , $c = 1, \dots, n$, with our spatial monotone model described in Section 1.2. Setting the first-stage parameterization of the risk function $f_c(\mathbf{X}_c) = \mathbf{b}_c(\mathbf{X}_c)\beta_c$ equal to the second-stage parameterization $f_c(\mathbf{X}_c) = \mathbf{B}(\mathbf{X}_c)\mathbf{T}^{-1}\theta_c$ and solving for β_c yields $\beta_c = \mathbf{A}_c\theta_c$, where

$$(10) \quad \mathbf{A}_c = [\mathbf{b}_c^T(\mathbf{X}_c)\mathbf{b}_c(\mathbf{X}_c)]^{-1}\mathbf{b}_c^T(\mathbf{X}_c)\mathbf{B}(\mathbf{X}_c)\mathbf{T}^{-1}.$$

The quantity $\mathbf{A}_c\theta_c$ is the projection of the second-stage log risk surface onto the column space of the first-stage basis expansion.

Most two-stage approaches use the likelihood $\hat{\beta}_c \sim N(\beta_c, \hat{\mathbf{V}}_{c,11})$ in the second stage, where $\hat{\beta}_c$ and $\hat{\mathbf{V}}_c$ are the first-stage estimates of β_c and \mathbf{V}_c [e.g., Dominici et al. (2002), Bell et al. (2004)]. For our model β_c does not have the same meaning in each city. We instead replace β_c with $\mathbf{A}_c\theta_c$ and use the second-stage likelihood

$$(11) \quad \left(\begin{array}{c} \hat{\beta}_c \\ \hat{\gamma}_c \end{array} \right) \middle| \theta_c, \gamma_c, \hat{\mathbf{V}}_c \sim N \left[\left(\begin{array}{c} \mathbf{A}_c\theta_c \\ \gamma_c \end{array} \right), \hat{\mathbf{V}}_c \right].$$

To complete the second-stage model, we put a flat prior on γ and use the prior model described in Section 1.2 for θ^* (and thus for θ).

2.3. Priors and computational details. We estimate (1) with quasi-likelihood methods and the `glm` function in R to obtain the first-stage parameter estimates $\hat{\beta}_c$, $\hat{\gamma}_c$ and $\hat{\mathbf{V}}_c$, for $c = 1, \dots, N$, where $\hat{\mathbf{V}}_c$ is the covariance matrix based on the Fisher's information matrix returned from the `glm` package. We use an offset proportional to the log population to account for different population sizes. To complete the Bayesian specification of the second-stage model, we use the hyperpriors:

$$(12) \quad \begin{aligned} \mu_0 &\sim N(0, \tau_0^2), \\ \mathbf{S}_2 &\sim \text{IW}(M_2 + 2, \mathbf{I}), \\ \mathbf{S}_1 &\sim \text{IW}(M_1 + 2, \mathbf{I}), \\ \tau &\sim \text{Ga}(a_\tau, b_\tau) \quad \text{and} \\ \log(\rho) &\sim N(\mu_\rho, \sigma_\rho^2). \end{aligned}$$

We are interested in the posterior of $(\boldsymbol{\theta}_c^T, \boldsymbol{\gamma}_c^T)^T$. To expedite computation, we perform MCMC sampling on the marginal posterior of $\boldsymbol{\theta}_c$, marginalizing over $\boldsymbol{\gamma}_c$ which is immediate from (11).

The parameters $\boldsymbol{\mu}$, μ_0 , τ , \mathbf{S}_1 and \mathbf{S}_2 have simple conjugate forms and are updated with Gibbs sampling. The latent $\boldsymbol{\theta}_c^*$ are sampled with a Gibbs sampler using a mixture of truncated normals. The range does not have a closed-form full conditional. We sample $\log(\rho)$ with a random-walk Metropolis–Hastings sampler. The full conditional for all parameters, acceptance ratio for ρ and MCMC algorithm are provided in supplementary material, Appendix D [Wilson et al. (2014)].

To get the predicted values used for cross-validation in Section 3.1, we need the posterior mean of $\boldsymbol{\gamma}_c$,

$$(13) \quad \mathbb{E}(\boldsymbol{\gamma}_c | \boldsymbol{\theta}_c, \hat{\boldsymbol{\beta}}_c, \hat{\boldsymbol{\gamma}}_c, \mathbf{V}_c) = \hat{\boldsymbol{\gamma}}_c + \mathbf{V}_{c,21} \mathbf{V}_{c,11}^{-1} (\mathbf{A}_c \bar{\boldsymbol{\theta}}_c - \hat{\boldsymbol{\beta}}_c),$$

where $\bar{\boldsymbol{\theta}}_c$ is the posterior mean of $\boldsymbol{\theta}_c$. Hence, no MCMC is required to get the posterior mean of $\boldsymbol{\gamma}_c$, rather, it can be computed in closed form using the marginal posterior estimate.

3. Analysis of the ozone-temperature log RR surfaces. In this section we estimate the city-specific and national average log RR surfaces using the two-stage approach presented in Section 2 and examine the nature of the ozone effect at different temperatures and ozone levels. We use the NMMAPS data and estimate the risk surfaces using same-day 1-hour maximum ozone and mean temperature, and estimate the surfaces for the same 95 US urban areas used in Bell et al. (2004). The NMMAPS data contains time-series data for 1987 through 2000 with daily mortality counts by age group and daily measurements of ozone, meteorological conditions and co-pollutants. We limit the analysis to April through October, or ozone season.

3.1. Cross-validation. We performed cross-validation to determine if the spatial monotone risk surface model fits the data better than alternative models and to determine the order of polynomials to use. For each city we used 80% of the data as a training set and fit each model to those data. We compared models with the deviance of the 20% holdout sample using the predicted values. The cross-validation deviance is $2[\hat{Y}_{ct} - Y_{ct} \log(\hat{Y}_{ct}) - \log(Y_{ct}!)]$, where \hat{Y}_{ct} is the predicted mortality count on holdout sample day t in city c .

The comparison models are as follows:

- (1) A nonspatial monotone risk surface model that replaces the multivariate Gaussian process on $\boldsymbol{\theta}_c^*$ with an independent multivariate normal model at each site. Hence, $\boldsymbol{\theta}_c^*$ are independent $N(\boldsymbol{\mu}, \mathbf{S}_2 \otimes \mathbf{S}_1)$.

(2) A spatial unconstrained risk surface version that models $f(\mathbf{x}; \boldsymbol{\theta}_c)$ directly with a (nontruncated) multivariate Gaussian process prior for $\boldsymbol{\theta}_c$, hence removing the monotonicity constraint.

(3) A nonspatial unconstrained model that combines the two previously described simplifications of the monotone risk surface model.

(4) The NMMAPS model presented in Bell et al. (2004) with a linear ozone effect and natural spline for temperature.

(5) An additive model that replaces the linear ozone effect in the NMMAPS model with an unconstrained spline.

For the risk surface models we use the noninformative hyperparameters $\tau_0 = 100$, $a_\tau = 0.001$ and $b_\tau = 0.001$. For the range parameter we let $\mu_\rho = 7$ and $\sigma_\rho = 10$ to provide a diffuse prior centered around 1000 km, which is about the range estimate reported in Smith, Xu and Switzer (2009). For the additive model we use the same priors formulation as the nonspatial, unconstrained model, but only use a basis expansion of ozone in f_c since temperature is accounted for in the confounder model. The second-stage model was run for 500,000 iterations and the first half were discarded as burn-in. We thinned the posterior sample, keeping every 50th draw due to high autocorrelation, primarily in the range parameter. Figures 4 and 5 in the supplementary material show trace plots of the posterior sample used for analysis [Wilson et al. (2014)].

Table 1 shows the difference in cross-validation deviance from the NMMAPS model for the other five models. For the spatial monotone model the best performing model had second-stage expansion of order $M_1 = 7$ and $M_2 = 9$ and first-stage city-specific expansion orders $M_1^c = \max(r_1^c M_1 / r_1, 6)$ and $M_2^c = \max(r_2^c M_2 / r_2, 4)$. Hence, the first-stage expansions are smaller and proportional to the ratio of the city-specific range (r_l^c) to the national range (r_l) down to a minimum order. CV results for this order are presented in Table 1. Additional results for other order expansions are provided in Appendix B in the supplementary material [Wilson et al. (2014)].

TABLE 1
Difference in cross-validation deviance from the linear additive model (NMMAPS model)

	Overall	Above 95th percentile		
		Ozone	Temperature	Both
Spatial monotone	−473.2	−42.3	−38.7	−21.1
Nonspatial monotone	−459.9	−40.2	−38.5	−20.7
Spatial unconstrained	−461.4	−38.0	−35.7	−18.9
Nonspatial unconstrained	−447.9	−38.0	−39.5	−21.4
Additive ($M_1 = 4$)	−353.9	−24.6	−28.7	−16.5

Overall, the spatial monotone model has the smallest cross-validation deviance. All four risk surface models have deviances well below those of the linear and nonlinear additive models. Hence, the data support using a non-additive, nonlinear model. About one-third of the difference between the spatial monotone and spatial unconstrained risk surface models is in the high ozone area where there is less data and the signal can be weak. The monotonicity constraint helps inform the model and reduces variance in the tails while making a relatively smaller difference over the areas with richer data. In addition, the monotonicity constraint smooths the risk surfaces because there cannot be mini peaks and valleys in the surface. This too helps improve fit in the holdout data set and it seems reasonable to assume the exposure response relationship should be fairly smooth. Because we are interested in the tail behavior, we compare the deviance on holdout sample days with ozone above each city's 95th percentile, days with temperature above the 95th percentile and the intersection of the two. The spatial monotone model had the lowest deviance for higher ozone, but the nonspatial unconstrained model fit slightly better for high temperature and the intersection. We proceed to analyze the data with the spatial monotone model with $M_1 = 7$ and $M_2 = 9$.

3.2. Analysis of the national average log RR surface. The national ozone-temperature log RR surface (the derivative of f with respect to ozone) shows an association between daily 1-hour maximum ozone and mortality with posterior probability greater than 0.99. The ozone effect is greater at higher ozone concentrations and at higher temperatures. Hence, a one ppb increase in ozone is associated with a larger increase in mortality on high temperature days and days with higher ozone levels. Figure 2(a) shows the national log RR surface plotted over the range of observed data. This is the pointwise average over the city-specific log RR surfaces weighted by the pointwise city-specific precision. Figure 2(c) and (d) show the log RR of ozone at 50 ppb and 100 ppb, respectively, as functions of temperature, along with 95% posterior intervals. All results for log RR are the gradient (3) multiplied by 1000. This can be interpreted as the expected percent change in mortality associated with a 10 ppb increase in ozone, where 10 ppb was chosen to be consistent with other publications.

At higher ozone concentrations, temperature has a larger modifying effect. Figure 3 shows the log RR at the 50th, 75th, 95th, and 99th percentiles of temperature as a function of ozone. For each temperature, log RR increases at higher ozone concentrations. As temperature increases from the median, the log RR increases monotonically for all ozone values, however, the difference between the cross-sections at low ozone values is very small. The posterior probability that RR is greater at the 99th percentile than the 50th percentile is about 0.92 [Figure 3(b)].

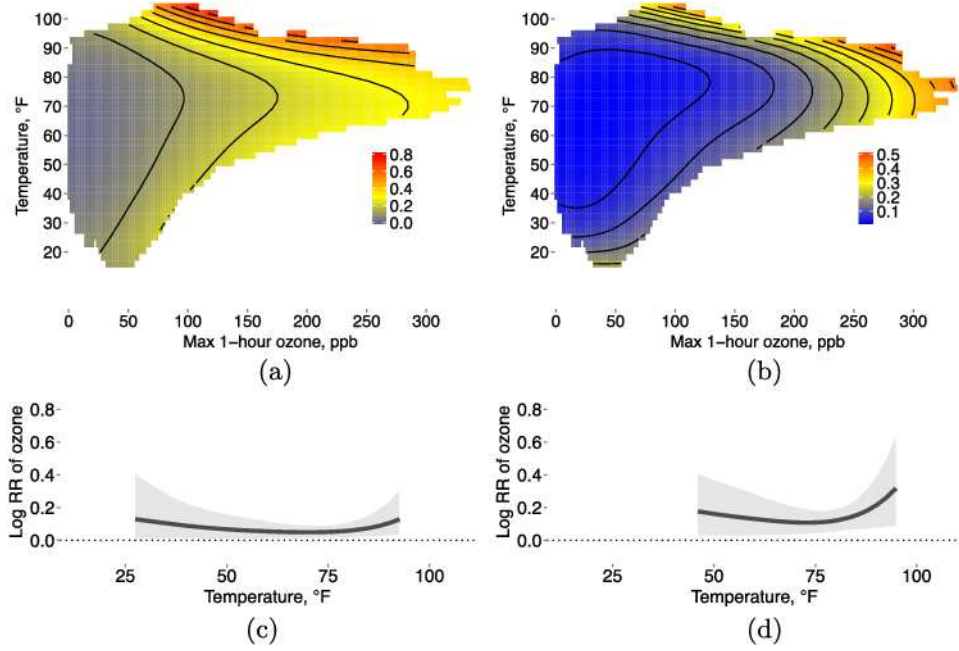


FIG. 2. Panels (a) and (b) show the pointwise mean and standard deviation of the national log RR surfaces. Panels (c) and (d) show a cross section of the log RR surface with ozone fixed at 50 and 100 ppb, respectively, along with 95% posterior intervals. Log RR is in percent change in mortality per one ppb increase in ozone.

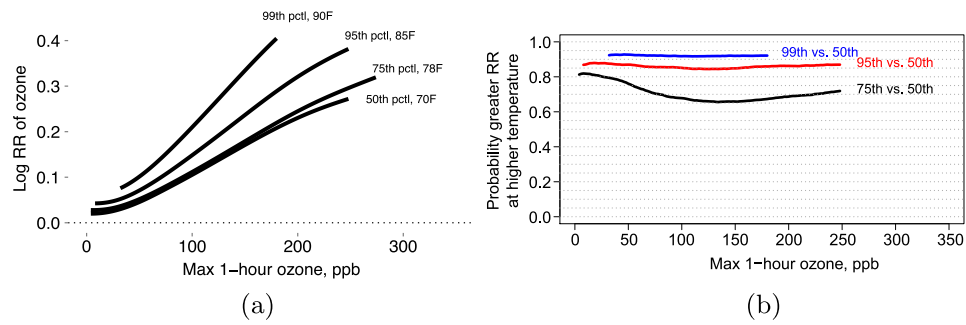


FIG. 3. Comparison of the log RR at the 50th, 75th, 95th and 99th percentiles of temperature. The estimates are plotted over the range of ozone values observed at that temperature in at least 5 cities. (a) Shows the mean log RR for each cross section and (b) shows the pointwise posterior probability that log RR is greater at the high temperature. Log RR is in percent change in mortality per one ppb increase in ozone. (a) Mean log RR for four percentiles of temperature (50th, 75th, 95th, 99th), (b) posterior probability that RR is greater at higher temperatures than median temperatures for each ozone value.

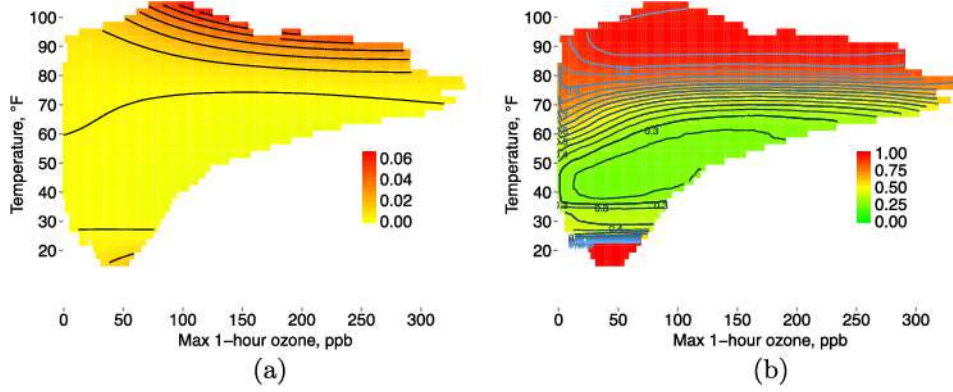


FIG. 4. National interaction surface and pointwise posterior probability of positive interaction. (a) Shows the national interaction surface which is the cross-derivative of the log risk surface or the derivative of the log RR surface with respect to temperature. This shows how log RR changes with temperature and quantifies the interaction at each point. (b) Shows the posterior probability that the national interaction surface is greater than 0.

The cross-derivative of the risk surface provides a more complete picture of a departure from additivity. The cross-derivative surface is

$$(14) \quad \frac{\partial^2 f_c(\mathbf{x})}{\partial x_1 \partial x_2} = M_1 M_2 \sum_{j=0}^{M_1-1} \sum_{k=0}^{M_2-1} (\theta_{j,k+1,c} - \theta_{j,k,c}) B_{j,k}(\mathbf{x}, M_1 - 1, M_2 - 1).$$

We refer to (14) as the interaction surface, as it is the rate of change in the log RR surface with respect to temperature. With an additive model the cross-derivative is zero. Figure 4 shows the national interaction surface and the pointwise posterior probability that the interaction is greater than zero. The national interaction surface shows a synergistic effect at higher ozone and temperatures. This synergism occurs with a posterior probability greater than 0.95 over the part of the surface with temperature equal to 90°F. At lower temperatures, the mean interaction is negative, although not with a high posterior probability in this summer-only analysis.

3.3. Analysis of the city-specific log RR surfaces. We now examine the city-specific surfaces and interaction at the city level. Figure 5 shows examples of four city-specific log RR surfaces and their pointwise standard deviations. While the national log RR surface shows a high posterior probability of a positive ozone effect, the city-specific ozone effect, averaged over the observed days in each city, is positive with posterior probability greater than 0.95 in six cities (Los Angeles, CA; Dallas/Ft. Worth, TX; Houston, TX; San Jose, CA; Oakland, CA; and St. Louis, MO).

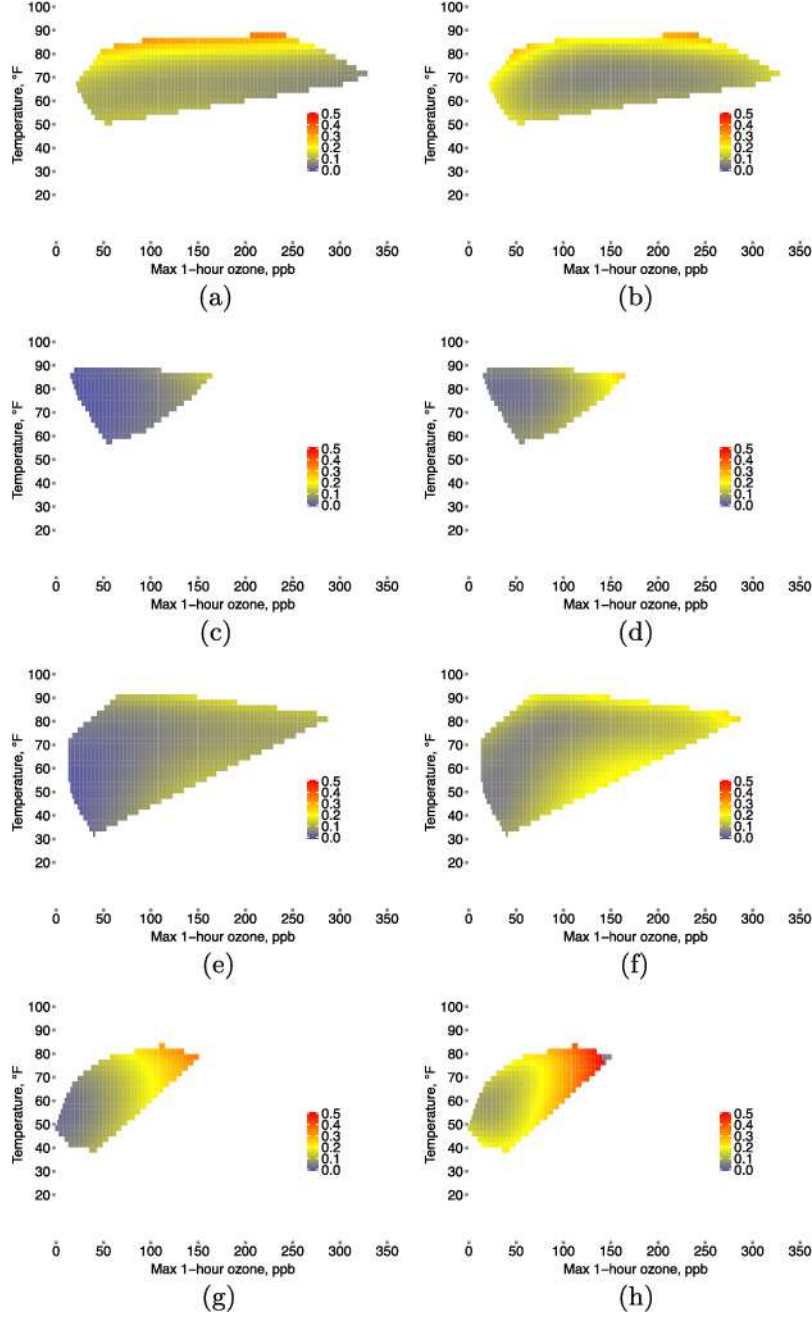


FIG. 5. *Log RR surfaces for selected cities (left) and their pointwise standard deviations (right). Surfaces are plotted only over the range of data observed data for that city. The cities were selected for being geographically diverse and having varied ozone and temperature ranges. (a) Los Angeles log RR surface, (b) Los Angeles SD, (c) Miami log RR surface, (d) Miami SD, (e) New York log RR surface, (f) New York SD, (g) Seattle log RR surface, (h) Seattle SD.*

To evaluate the interaction effect, we compare high and moderate temperature days in each city. We define high temperature days as those with temperatures between the 95th and 99th city-specific temperature percentiles and moderate temperature days to have temperatures between the 50th and 75th percentiles. Within each range we include only days between the 10th and 90th percentiles of ozone in order to minimize the influence of days with extreme ozone values in either direction. Figure 1 outlines these days in black for four cities. By using city-specific percentiles this definition of high and moderate temperature days adapts to each city’s weather; however, like previous studies that used a stratified model to compare log RR at different temperatures, it does not account for the different ozone distributions of high and moderate temperature days. To remove the effect of different ozone ranges, we limit the high and moderate temperature regions to a common ozone range, indicated by the purple box in Figure 1.

On high temperature days the log RR is larger than on moderate temperature days over the observed ozone range in most cities, but the difference is greatly reduced when comparing only over the common ozone range. Figure 6 compares the ratio of mean log RR on high temperature days to mean log RR on moderate temperature days for both ozone ranges. The large reduction in the ratio when limiting to a common ozone range suggests that much of the difference in log RR between high and moderate temperature days is due to the higher ozone levels on high temperature days in conjunction with the nonlinearity of the ozone effect. Over the common ozone range, the ratio ranged from about 1 to 2.5. Most of the cities with larger levels of interaction over the common ozone range are in the north where there is a larger difference between the temperatures on high and moderate temperature days (Figure 7 and Table 2).

These results are similar to many previous studies that find statistical significance at the national level but in only a handful of cities [see Bell et al. (2004), e.g.]. The motivation of hierarchical modeling and sharing information between cities in our study is to increase the power to estimate effects. While the posterior probabilities in most cities do not strongly support interaction at the city level, the city-specific point estimates imply interaction in many cities, a result consistent with the national results presented in Section 3.2.

3.4. Analysis of excess mortality. Overall we see a trend of a synergistic ozone-temperature effect, both in the national log RR surface and interaction surface, and in the city-specific estimates. This interaction at higher ozone levels and temperatures leads to a larger estimate of excess mortality.

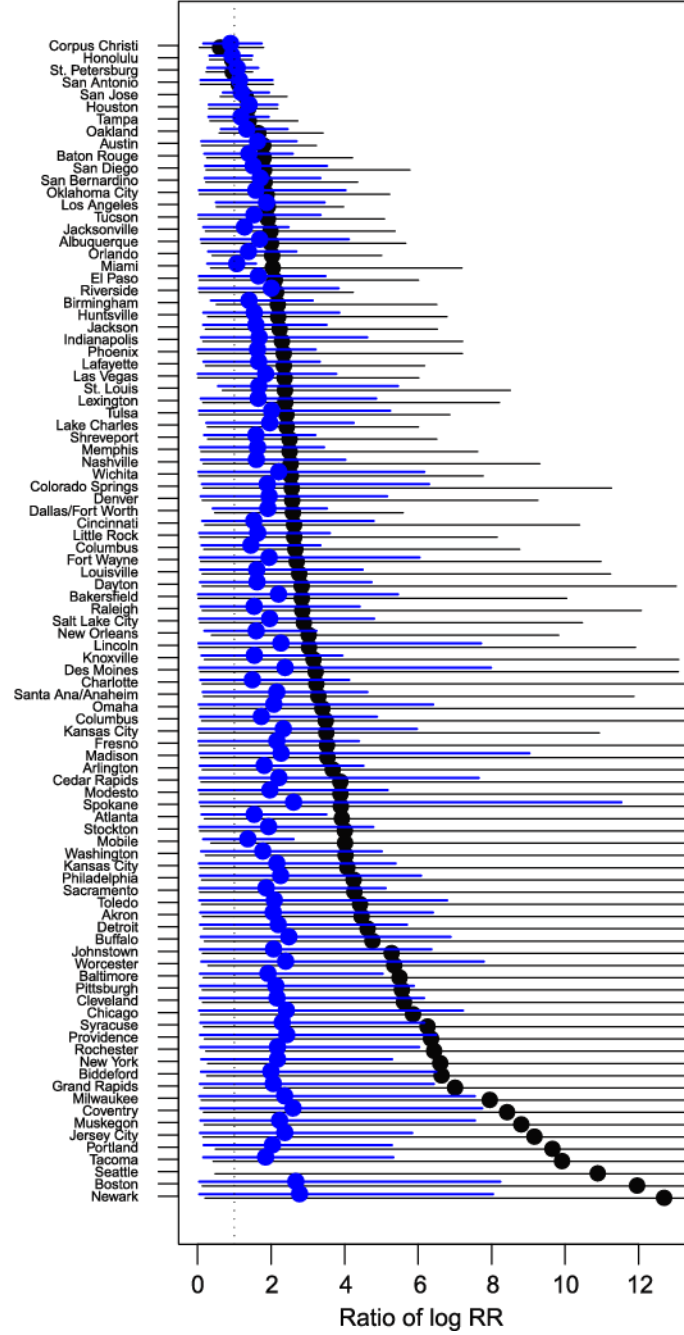


FIG. 6. Comparison of the log RR at high temperatures and moderate temperatures as defined in Section 3.3. The ratio of log RR over the observed ozone range is shown in black and common ozone range is in blue. The posterior mean and 95% interval are shown.

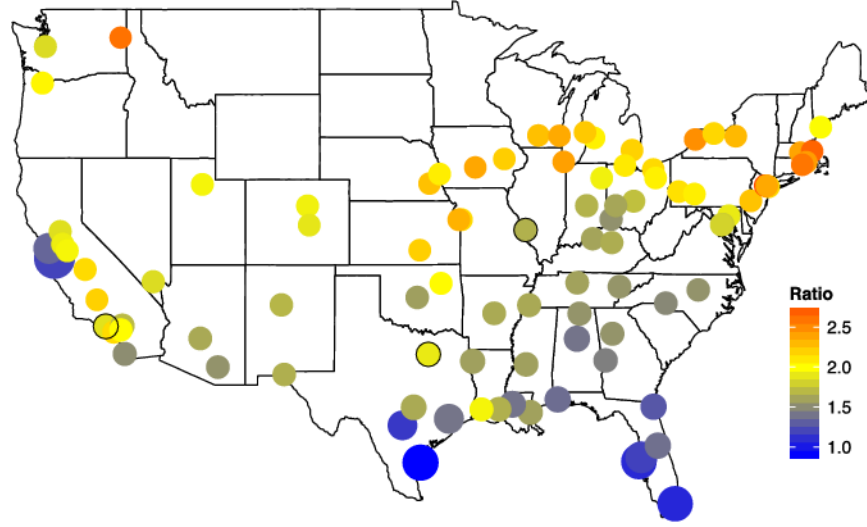


FIG. 7. Map of the ratio of log RR at high temperatures and moderate temperatures over the common ozone range as defined in Section 3.3. The RR at higher temperatures is greater than the RR at moderate temperatures with posterior probability at least 0.8 in the cities outlined in black (Dallas/Ft. Worth, Los Angeles, and St. Louis).

Table 3 compares the expected change in mortality associated with an increase from median ozone and temperature to the 95th percentile of ozone and temperature for the additive linear model (NMMAPS), the additive nonlinear model and the monotone, spatial risk surface model by region. The general trends are the same, with the largest effects observed in the

TABLE 2
Mean log RR on high and moderate temperature days over the observed and common ozone rates by region (in percent change in mortality per 10 ppb increase in ozone)

	Observed ozone range		Common ozone range	
	High temp.	Moderate temp.	High temp.	Moderate temp.
Indust. midwest	0.25 (0.10)	0.17 (0.06)	0.24 (0.09)	0.19 (0.07)
Northeast	0.12 (0.09)	0.06 (0.05)	0.11 (0.09)	0.07 (0.05)
Northwest	0.14 (0.06)	0.07 (0.03)	0.12 (0.05)	0.09 (0.04)
Southern CA	0.13 (0.07)	0.08 (0.05)	0.11 (0.06)	0.09 (0.06)
Southeast	0.17 (0.39)	0.14 (0.33)	0.17 (0.39)	0.15 (0.33)
Southwest	0.14 (0.08)	0.08 (0.05)	0.13 (0.08)	0.08 (0.05)
Upper midwest	0.10 (0.07)	0.06 (0.04)	0.09 (0.07)	0.06 (0.04)
National	0.15 (0.04)	0.09 (0.02)	0.13 (0.04)	0.10 (0.03)

Note: The regions from the NMMAPS data are used [see Samet et al. (2000a, 2000b)].

TABLE 3
Percent increase in mortality associated with an increase from the medians of ozone and temperature to the 95th percentiles of ozone and temperature using different models

	Additive linear	Additive nonlinear	Surface
Indust. midwest	4.57 (0.77)	3.27 (1.65)	4.13 (0.42)
Northeast	5.61 (0.94)	5.88 (1.92)	5.31 (0.48)
Northwest	3.92 (0.82)	0.90 (1.84)	2.42 (0.58)
Southern CA	2.77 (0.80)	3.89 (2.57)	3.88 (0.77)
Southeast	0.70 (0.52)	3.15 (1.20)	3.23 (0.38)
Southwest	2.89 (0.84)	4.71 (2.04)	4.49 (0.64)
Upper midwest	1.33 (1.21)	2.91 (2.08)	4.82 (0.62)
National	3.06 (0.30)	3.54 (0.75)	3.98 (0.24)

industrial midwest, but the risk surface estimates are more homogeneous across regions.

4. Discussion. In this paper we propose a two-stage procedure to estimate city-specific ozone-temperature risk surfaces. To accommodate different temperature and ozone ranges in different cities, we use local basis expansions in the first stage. The first-stage results are combined in the second-stage model using a global basis expansion and spatially-varying coefficients to allow for different ozone-temperature effects by city.

We evaluated the model fit with respect to the modeling assumptions using cross-validation and the results indicated that monotonically nondecreasing shape-restricted ozone effect in a spatial model was best supported by the data. These results suggest that the monotonic constraint helps inform the model where data is sparse while allowing the constraints of linearity of the association to be relaxed. Previous attempts to analyze the bivariate effect of temperature and ozone on mortality have either over-smoothed with loss of information on potential interaction or under-smoothed, resulting in biologically implausible scenarios where increasing doses of ozone may alternate between being beneficial and detrimental to health [Cheng and Kan (2012), Burkart et al. (2013), Ren et al. (2008a, 2008b)].

Our analysis of the data in 95 US cities provides additional evidence that the effects of ozone and temperature are nonlinear, and depart from simple additivity between ozone and temperature. Specifically, the national average log RR surface indicates that the RR of ozone is higher on high temperature days and this interaction is most pronounced in the northern US, where summer temperatures have the most variability.

The results of this study have important implications toward understanding the nature of the joint effects of ozone and temperature on mortality.

To compare the ozone effect between different temperature strata, it is important that the distributions of ozone be similar within each strata. High correlation between temperature and ozone violate this requirement and thus call for careful consideration and interpretation of methods. Indeed, the results suggest that the higher ozone estimates at high temperatures in stratified studies are primarily due to the nonlinear effect of ozone coupled with higher concentrations of ozone formed at high temperatures. However, the results also suggest that modification of risk is present at higher temperature levels.

IPCC (2007) raised concerns about whether current air quality management practices can adequately protect public health under the future climate regimes. Climate projections show increases in extreme ozone and temperature days over a significant portion of the US [Hogrefe et al. (2004), Kunkel et al. (2008), Tagaris et al. (2007), Wu et al. (2008)]. The synergistic ozone-temperature effect estimated in this paper implies that the disease burden of these extreme weather days is greater than would be estimated with additive models. This is despite the relatively small size of the interaction effect compared to the nonlinear main effect at higher ozone levels.

In our paper we have developed methodology to capture nonlinear interactions between temperature and ozone effects. This methodology could be used in other health effects analyses and potentially beyond. For example, there is increasing interest in identifying joint effects of multiple pollutants [National Research Council (2004)]. Recent work on multiple-pollutant modeling include Kalendra (2010) and Bobb, Dominici and Peng (2013), who study the joint effect of ozone and fine particulate matter. Another application is studying cumulative effects using various lagged pollution or temperature variables [Heaton and Peng (2012, 2014), Schwartz (2000), Welty and Zeger (2005)]. Bell et al. (2004) found that the current day ozone exposures (lag 0), the same measure analyzed in this paper, have the largest effect on total mortality and cardiovascular and respiratory deaths. However, previous day exposures (lags 1 and 2) were also significantly associated with daily mortality, as was the cumulative effect of exposures of the previous week (lags 0–6). For any two predictors our method would apply directly; extending the model to include a high-dimensional surface for the joint effect of several predictors will be challenging. To accommodate several predictors, our approach could be modified to have an additive structure [Hastie and Tibshirani (1990)] with main effect curves for each predictor and two-dimensional interaction surfaces for pairs of variables thought to interact.

SUPPLEMENTARY MATERIAL

Appendices (DOI: [10.1214/14-AOAS754SUPP](https://doi.org/10.1214/14-AOAS754SUPP); .pdf). Appendices referenced in the text are provided in the supplementary appendix file [Wilson

et al. (2014)]. Appendix A: additional figures. Appendix B: cross-validation results. Appendix C: full conditional distributions. Appendix D: MCMC algorithm. Appendix E: trace plots.

REFERENCES

- BANERJEE, S., GELFAND, A. E. and CARLIN, B. P. (2004). *Hierarchical Modeling and Analysis for Spatial Data*. CRC Press, Boca Raton, FL.
- BELL, M. L. and DOMINICI, F. (2008). Effect modification by community characteristics on the short-term effects of ozone exposure and mortality in 98 US communities. *Am. J. Epidemiol.* **167** 986–997.
- BELL, M. L., PENG, R. D. and DOMINICI, F. (2006). The exposure-response curve for ozone and risk of mortality and the adequacy of current ozone regulations. *Environ. Health Perspect.* **114** 532–536.
- BELL, M. L., McDERMOTT, A., ZEGER, S. L., SAMET, J. M. and DOMINICI, F. (2004). Ozone and short-term mortality in 95 US urban communities, 1987–2000. *J. Am. Med. Assoc.* **292** 2372–2378.
- BHASKARAN, K., HAJAT, S., HAINES, A., HERRETT, E., WILKINSON, P. and SMEETH, L. (2009). Effects of ambient temperature on the incidence of myocardial infarction. *Heart* **95** 1760–1769.
- BLOOMER, B. J., STEHR, J. W., PIETY, C. A., SALAWITCH, R. J. and DICKERSON, R. R. (2009). Observed relationships of ozone air pollution with temperature and emissions. *Geophys. Res. Lett.* **36**.
- BOBB, J. F., DOMINICI, F. and PENG, R. D. (2013). Reduced hierarchical models with application to estimating health effects of simultaneous exposure to multiple pollutants. *J. R. Stat. Soc. Ser. C. Appl. Stat.* **62** 451–472. [MR3060626](#)
- BURKART, K., CANÁRIO, P., BREITNER, S., SCHNEIDER, A., SCHERBER, K., ANDRADE, H., ALCOFORADO, M. J. and ENDLICHER, W. (2013). Interactive short-term effects of equivalent temperature and air pollution on human mortality in Berlin and Lisbon. *Environ. Pollut.* **183** 54–63.
- CHANG, I.-S., CHIEN, L.-C., HSIUNG, C. A., WEN, C.-C. and WU, Y.-J. (2007). Shape restricted regression with random Bernstein polynomials. In *Complex Datasets and Inverse Problems. Institute of Mathematical Statistics Lecture Notes—Monograph Series* **54** 187–202. IMS, Beachwood, OH. [MR2459189](#)
- CHEN, K., YANG, H. B., MA, Z. W., BI, J. and HUANG, L. (2013). Influence of temperature to the short-term effects of various ozone metrics on daily mortality in Suzhou, China. *Atmos. Environ.* **79** 119–128.
- CHENG, Y. and KAN, H. (2012). Effect of the interaction between outdoor air pollution and extreme temperature on daily mortality in Shanghai, China. *J. Epidemiol.* **22** 28–36.
- CURRIERO, F. C., HEINER, K. S., SAMET, J. M., ZEGER, S. L., STRUG, L. and PATZ, J. A. (2002). Temperature and mortality in 11 cities of the eastern United States. *Am. J. Epidemiol.* **155** 80–87.
- CURTIS, S. M. and GHOSH, S. K. (2011). A variable selection approach to monotonic regression with Bernstein polynomials. *J. Appl. Stat.* **38** 961–976. [MR2782409](#)
- DOMINICI, F., DANIELS, M., ZEGER, S. L. and SAMET, J. M. (2002). Air pollution and mortality: Estimating regional and national dose-response relationships. *J. Amer. Statist. Assoc.* **97** 100–111. [MR1963390](#)
- GELFAND, A. E., DIGGLE, P. J., GUTTORP, P. and FUENTES, P. (2013). *Handbook of Spatial Statistics*. CRC Press, Boca Raton, FL.

- HASTIE, T. J. and TIBSHIRANI, R. J. (1990). *Generalized Additive Models. Monographs on Statistics and Applied Probability* **43**. Chapman & Hall, London. [MR1082147](#)
- HEATON, M. J. and PENG, R. D. (2012). Flexible distributed lag models using random functions with application to estimating mortality displacement from heat-related deaths. *J. Agric. Biol. Environ. Stat.* **17** 313–331. [MR2993269](#)
- HEATON, M. J. and PENG, R. D. (2014). Extending distributed lag models to higher degrees. *Biostatistics* **15** 398–412.
- HOGREFE, C., LYNN, B., CIVEROLO, K., KU, J.-Y., ROSENTHAL, J., ROSENZWEIG, C., GOLDBERG, R., GAFFIN, S., KNOWLTON, K. and KINNEY, P. L. (2004). Simulating changes in regional air pollution over the eastern United States due to changes in global and regional climate and emissions. *J. Geophys. Res., Atmospheres* **109**.
- HORSTMAN, D. H., FOLINSBEE, J. L., IVES, P. J., ABDUL-SALAAM, S. and McDONNELL, W. F. (1990). Ozone concentration and pulmonary response relationships for 6.6-hour exposures with five hours of moderate exercise to 0.08, 0.10, and 0.12 ppm. *Am. Rev. Respir. Dis.* **142** 1158–1163.
- IPCC, I. (2007). Fourth assessment report: Climate change 2007: Working group I report: The physical science basis. Technical report.
- KALENDRA, E. J. (2010). Space-time modeling of health effects while controlling for spatially varying exposure surfaces. Doctoral dissertation, Dept. of Statistics, North Carolina State Univ. (ID: NCSU2277462). [MR2941644](#)
- KORRICK, S. A., NEAS, L. M., DOCKERY, D. W., GOLD, D. R., ALLEN, G. A., HILL, L. B., KIMBALL, K. D., ROSNER, B. A. and SPEIZER, F. E. (1998). Effects of ozone and other pollutants on the pulmonary function of adult hikers. *Environ. Health Perspect.* **106** 93–99.
- KUNKEL, K., HUANG, H.-C., LIANG, X.-Z., LIN, J.-T., WUEBBLES, D., TAO, Z., WILLIAMS, A., CAUGHEY, M., ZHU, J. and HAYHOE, K. (2008). Sensitivity of future ozone concentrations in the northeast USA to regional climate change. *Mitig. Adapt. Strategies Glob. Change* **13** 597–606.
- LAWSON, A. B. (2006). *Statistical Methods in Spatial Epidemiology*. Wiley, Chichester.
- LORENTZ, G. G. (1986). *Bernstein Polynomials*, 2nd ed. Chelsea, New York. [MR0864976](#)
- MCDONNELL, W. F., STEWART, P. W., SMITH, M. V., KIM, C. S. and SCHELEGLE, E. S. (2012). Prediction of lung function response for populations exposed to a wide range of ozone conditions. *Inhal. Toxicol.* **24** 619–633. PMID: 22906168.
- NATIONAL RESEARCH COUNCIL (2004). Research priorities for airborne particulate matter: IV, continuing research progress. Technical report, National Research Council of the National Academies, Washington, DC.
- OSTRO, B. (1993). The association of air pollution and mortality: Examining the case for inference. *Archives of Environmental Health: An International Journal* **48** 336–342. PMID: 8215598.
- REN, C., WILLIAMS, G. M., Mengersen, K., MORAWSKA, L. and TONG, S. (2008a). Does temperature modify short-term effects of ozone on total mortality in 60 large eastern US communities?—An assessment using the nmmaps data. *Environ. Int.* **34** 451–458.
- REN, C., WILLIAMS, G. M., MORAWSKA, L., Mengersen, K. and TONG, S. (2008b). Ozone modifies associations between temperature and cardiovascular mortality: analysis of the nmmaps data. *Occup. Environ. Med.* **65** 255–260.
- SAMET, J. M., DOMINICI, F., ZEGER, S. L., SCHWARTZ, J. and DOCKERY, D. W. (2000a). *The National Morbidity, Mortality, and Air Pollution Study Part I: Methods and Methodologic Issues*. Health Effects Institute, Cambridge, MA.

- SAMET, J. M., DOMINICI, F., ZEGER, S. L., SCHWARTZ, J. and DOCKERY, D. W. (2000b). *The National Morbidity, Mortality, and Air Pollution Study Part II: Morbidity and Mortality from Air Pollution in the United States*. Health Effects Institute, Cambridge, MA.
- SCHWARTZ, J. (2000). The distributed lag between air pollution and daily deaths. *Epidemiology* **11** 320–326.
- SMITH, R. L., XU, B. and SWITZER, P. (2009). Reassessing the relationship between ozone and short-term mortality in U.S. urban communities. *Inhal. Toxicol.* **21** 37–61. PMID: 19731973.
- TAGARIS, E., MANOMAIPHIBOON, K., LIAO, K.-J., LEUNG, L. R., WOO, J.-H., HE, S., AMAR, P. and RUSSELL, A. G. (2007). Impacts of global climate change and emissions on regional ozone and fine particulate matter concentrations over the United States. *J. Geophys. Res., Atmospheres* **112**.
- TENBUSCH, A. (1997). Nonparametric curve estimation with Bernstein estimates. *Metrika* **45** 1–30. [MR1437794](#)
- TURNER, L. R., BARNETT, A. G., CONNELL, D. and TONGA, S. (2012). Review article: Ambient temperature and cardiorespiratory morbidity: A systematic review and meta-analysis. *Epidemiology* **23** 594–606.
- US EPA (2006). Air quality criteria for ozone and related photochemical oxidants (2006 final). Technical Report EPA/600/R-05/004aF-cF, US Environmental Protection Agency, Washington, DC.
- US EPA (2009). Assessment of the impacts of global change on regional US air quality: A synthesis of climate change impacts on ground-level ozone (an interim report of the US EPA Global Change Research Program). Technical Report MSU-CSE-00-2, US Environmental Protection Agency, Washington, DC.
- US EPA (2013). Integrated science assessment of ozone and related photochemical oxidants (final report). Technical Report EPA/600/R-10/076F, US Environmental Protection Agency, Washington, DC.
- WANG, J. and GHOSH, S. K. (2012). Shape restricted nonparametric regression with Bernstein polynomials. *Comput. Statist. Data Anal.* **56** 2729–2741. [MR2915158](#)
- WELTY, L. J. and ZEGER, S. L. (2005). Are the acute effects of particulate matter on mortality in the national morbidity, mortality, and air pollution study the result of inadequate control for weather and season? A sensitivity analysis using flexible distributed lag models. *Am. J. Epidemiol.* **162** 80–88.
- WILSON, A., RAPPOLD, A., NEAS, L. and REICH, B. (2014). Supplement to “Modeling the effect of temperature on ozone-related mortality.” DOI:[10.1214/14-AOAS754SUPP](#).
- WU, S., MICKLEY, L. J., LEIBENSPERGER, E. M., JACOB, D. J., RIND, D. and STREETS, D. G. (2008). Effects of 2000–2050 global change on ozone air quality in the United States. *J. Geophys. Res., Atmospheres* **113**.

A. WILSON
B. J. REICH
DEPARTMENT OF STATISTICS
NORTH CAROLINA STATE UNIVERSITY
2311 STINSON DRIVE
RALEIGH, NORTH CAROLINA 27695
USA
E-MAIL: ander_wilson@ncsu.edu
brian_reich@ncsu.edu

A. G. RAPPOLD
L. M. NEAS
ENVIRONMENTAL PUBLIC HEALTH DIVISION
US ENVIRONMENTAL PROTECTION AGENCY
CHAPEL HILL, NORTH CAROLINA 27599
USA
E-MAIL: rappold.ana@epa.gov
neas.lucas@epa.gov